Available online at www.sciencedirect.com
SCIENCE DIRECT®
Carbon 43 (2005) 1936–1943
CARBON
www.elsevier.com/locate/carbon

A carbon activation model with application to longan seed char gasification

S. Junpirom [a], D.D. Do [c,*], C. Tangsathitkulchai [a], M. Tangsathitkulchai [b]

[a] School of Chemical Engineering, Suranaree University of Technology, Nakhon Ratchasima 30000, Thailand
[b] School of Chemistry, Suranaree University of Technology, Nakhon Ratchasima 30000, Thailand
[c] Department of Chemical Engineering, University of Queensland, St. Lucia, Brisbane, Qld 4072, Australia

Received 23 August 2004; accepted 1 March 2005
Available online 14 April 2005

Abstract

In this paper a new structural model is presented to describe the evolution of porosity of char during the gasification process. The model assumes the char structure to be composed of bundles of parallel graphite layers, and the reactivities of each layer with the gasification agent are assumed to be different to represent the different degree of heterogeneity of each layer (i.e. each layer will react with the gasification agent at a different rate). It is this difference in the reactivity that allows micropores to be created during the course of gasification. This simple structural model enables the evolution of pore volume, pore geometrical surface area and the pore size distribution to be described with respect to the extent of char burn-off. The model is tested against the experimental data of gasification of longan seed-derived char with carbon dioxide and it is found that the agreement between the model and the data is reasonably satisfactory, especially the evolution of surface area and pore volume with burn-off.

Keywords: Activated carbon; Gasification; Modeling; Porosity

1. Introduction

Activated carbon is commonly used as an adsorbent in many separation and purification systems. One of the reasons for its wide application is the very high specific surface area of activated carbon (typically in the order of 1000 $m^2 g^{-1}$), which is a prerequisite for achieving high adsorption capacity. Commercial activated carbon can be produced from a variety of carbonaceous materials employing either physical activation or chemical activation processes, with the former being more favorable. During the activation process, pores are created and developed (both in length and width), giving eventually a distribution of pore size. An understanding of how pores are developed during the activation process is an essential part in tailoring activated carbon with pore sizes suitable for the desired adsorption application. The reaction involved in the physical activation is the one between the carbon atom and the oxidizing gas. It is this reaction that gives rise to pore creation and development as some parts of the char structure are reacted faster than the others.

Characterization of resulting activated carbon is commonly carried out by studying adsorption isotherms of some common probe molecules. Adsorption equilibria in carbonaceous materials have been studied fairly intensively both experimentally and theoretically in the past few decades. This is mostly due to the advances in experimental techniques and the availability of high speed computer that make advanced theoretical tools such as density functional theory (DFT) [1] and Monte Carlo simulations [2–4] being applied more readily to solve numerous adsorption problems in carbon

* Corresponding author. Tel.: +61 7 3365 4154; fax: +61 7 3365 2789.
E-mail address: duongd@cheque.uq.edu.au (D.D. Do).

0008-6223/$ - see front matter © 2005 Elsevier Ltd. All rights reserved.
doi:10.1016/j.carbon.2005.03.001

materials. As a result of these studies, it is increasingly recognized that the pore size distribution [5–13] and the surface topology (including chemistry) [14] all affect the adsorption equilibria. Among these two factors, the pore size distribution is the prime factor when dealing with non-polar adsorbates or weakly polar adsorbates. Attempts to characterize a pore size distribution have been made by many workers in this field, mostly by using the measured adsorption isotherm and solving the integral equation of which the pore size distribution function is the kernel [15]. Such a derivation of pore size distribution depends on the appropriate choice of local isotherms which appear as the integrand of the above mentioned integral equation. In this paper, we will address this problem from the opposite direction, that is we model the process of char physical activation with either steam or carbon dioxide in an attempt to derive information on the evolution of geometrical surface area, pore volume and pore size distribution.

There are several models that have been developed in the literature to predict the porosity evolution of reacting solid. The modeling by treating the diffusion and reaction in a single cylindrical capillary and also in a random assembly of capillaries of the same radius was investigated by Petersen [16]. Szekely and Evans [17] used two structural models, pore model and grain model to explore the gas–solid reactions. Another approach employing population balance equations to describe the change in the pore structure during gasification process was proposed by Hashimoto and Silveston [18]. Gavalas [19] used a random capillary model to model char gasification. A random pore model for interpreting of fluid–solid reaction was developed by Bhatia and Perlmutter [20]. The discrete model was also used to illustrate the evolution of pore structure (Sandmann and Zygourakis [21]).

These models are mostly focused on the macroscopic properties of the solid. Such a picture does not properly describe the microscopic structure of char and the activated carbon product. It is the objective of this paper to develop a structural model that properly does so. In this proposed model, we simply assume that char is composed of bundles of graphite-like layers and the porosity is created via the consumption of carbon by the gasification reaction. The model results are validated with the experimental data of longan seed-derived char gasification by carbon dioxide. The longan seed, a potential precursor for activated carbon production, is an abundant solid waste produced from the fruit cannery.

2. Model description

It is well known that char produced from the carbonization process consists of amorphous carbon and graphitic crystallites [22,23]. The amorphous part is gasified during the initial stage of activation (burn-off <10%), giving rise to some pore creation by the opening of the original blocked pores. The next stage involves the gasification of graphite-like crystallites, which further creates new pores and widens existing pores. Since the gasification of amorphous carbon is too complex to model due to its highly disorganized structure, the model of char gasification proposed in this work will be limited to the gasification of the graphite-like crystallites. The contribution of pore creation by the amorphous carbon during the initial part of activation, as compared to that at higher burn-offs, is considered to be relatively small and this contribution can be incorporated into the crystallite model without appreciable error.

The carbon char is assumed to consist of bundles of graphite-like crystallites. Each of these crystallites contains equal-sized layers of carbon atoms, but each of these layers possesses different reactivity towards the gasifying agent as it is logical to expect physically that those layers are not energetically homogeneous with respect to chemical reaction. We use the random generator in MATLAB to generate randomly a number between zero and one to represent a reactivity for each of those layers or a group of layers. Such an assignment of random reactivity is consistent with the expectation of randomness in a realistic char particle. In our model, each crystallite contains fifteen carbon layers in accord with the experimental finding of Flanklin [24], and to ensure a good statistical averaging we use one hundred crystallites in the model system. A schematic diagram of one crystallite is shown in Fig. 1a.

The extent of gasification reaction for each carbon layer follows the reaction equation,

$$L_t = L_i - (a \times t), \tag{1}$$

where L_t is the length of carbon layer at a theoretical time t, L_i is the initial length of carbon layer, and a is the carbon layer reactivity, with the reaction progressing along the carbon plane in a lengthwise direction. In this model, the theoretical time is defined as an incremental integer starting from zero. The simulation is performed at each value of theoretical time to arrive at a certain value of burn-off along with the evaluated porous properties of the carbon, as follows. First, a reactivity number is randomly assigned to the carbon layer in each crystallite as a "layer group". The layer group designated as "1–n" group means that up to "n" adjacent layers of carbon are grouped together and all layers in that group have the same reactivity. For example, "1–1" group indicates that every carbon layer in a crystallite will have its own reactivity, "1–2" group means that some layers can have their own reactivity or two adjacent layers have the same reactivity, etc. The application of a layer group concept adds flexibility in controlling the micropore size distribution generated in

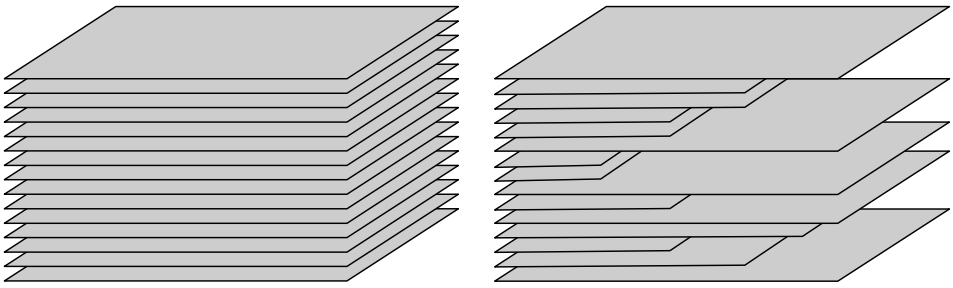

(a) A crystallite before activation (b) A crystallite after activation

Fig. 1. Schematic diagram of a graphitic crystallite.

the early stage of the gasification reaction. In this work, two types of layer group, 1–2 and 1–5 group, are selected for the simulation scheme. This would give the largest created pore width of 10 and 20 Å (based on an interlayer spacing of 3.35 Å of graphite), which constitute the micropore size range. Table 1 shows typical reactivity values for crystallite number 1–5 and number 96–100, showing layer groups of 1–2 and 1–5, respectively. To obtain good simulation results, it is also necessary to assign a zero reactivity to some of the crystallites to model the diffusional resistance inside the char in the early stage of gasification where the degree of burn-off is still low. Obviously, the number of these zero-reactivity crystallites decreases as the extent of reaction increases. For burn-off higher than 30%, the non-reactive crystallites are reassigned with reactivity numbers, and this situation represents kinetic-controlled gasification. The number of non-reactive crystallites used in the calculation and their relative importance up to 30% burn-off are arbitrarily selected and adjusted so that a good agreement between the experimental and computed porous properties of the char is obtained.

Next, from the theoretical time and the assigned reactivities, the linear length (L_t) of each carbon layer is calculated via Eq. (1). Using the interlayer spacing of 3.35 Å for graphite-like layers, the initial volume (V_0) and the volume of char at a theoretical time t (V) are calculated. The percentage burn-off of char is then calculated from the relation,

$$\%\text{burn-off} = [(V_0 - V)/V_0] \times 100 \quad (2)$$

The pore size and pore volume are estimated from the layer width and the void volume bound by two adjacent layers, respectively. The surface area for each pore size is then calculated from the area of the two opposite carbon planes. Pore volume distribution is readily obtained from the knowledge of pore volumes of different pore sizes. Fig. 1b illustrates the typical porous structure of the crystallite containing a number of slit pores at a given burn-off. The computation is repeated for larger values of theoretical time to give different degrees of

Table 1
Typical generated reactivities of carbon layers of some graphitic crystallites

Layer number	Crystallite number									
	1	2	3	4	5	96	97	98	99	100
1	0.034	0.704	0.333	0.092	0.967	0.937	0.772	0.126	0.499	0.926
2	0.100	0.704	0.333	0.092	0.654	0.012	0.772	0.126	0.499	0.926
3	0.528	0.149	0.117	0.393	0.111	0.694	0.772	0.126	0.499	0.926
4	0.356	0.149	0.117	0.393	0.657	0.795	0.772	0.126	0.755	0.926
5	0.823	0.718	0.138	0.035	0.386	0.339	0.772	0.228	0.755	0.926
6	0.240	0.718	0.138	0.035	0.004	0.956	0.024	0.228	0.755	0.137
7	0.979	0.130	0.420	0.458	0.685	0.346	0.024	0.228	0.526	0.137
8	0.797	0.130	0.420	0.458	0.855	0.532	0.024	0.228	0.526	0.137
9	0.828	0.680	0.917	0.930	0.396	0.184	0.024	0.117	0.526	0.137
10	0.560	0.680	0.917	0.930	0.317	0.640	0.024	0.117	0.332	0.137
11	0.369	0.779	0.784	0.071	0.198	0.855	0.385	0.117	0.332	0.218
12	0.853	0.779	0.784	0.071	0.756	0.199	0.385	0.117	0.332	0.218
13	0.229	0.764	0.486	0.724	0.162	0.434	0.385	0.907	0.750	0.218
14	0.119	0.764	0.486	0.724	0.136	0.435	0.385	0.907	0.750	0.218
15	0.965	0.231	0.513	0.980	0.131	0.272	0.385	0.907	0.750	0.218

burn-off and the corresponding porous properties of the gasified char. It should be noted that the application of the model to obtain a good fit between simulated and experimental results is based largely on the sensible selection of layer group pattern and the number of non-reactive carbon layers as previously described. The sum of square of relative error was used to evaluate the degree of fitting between the model results and the experimental data.

3. Experimental

3.1. Preparation of char

The fresh longan seed was washed in clean water and dried in the oven at 110 °C for 24 h. The pre-dried longan seed was crushed and sieved to obtain an average particle size of 2.1 mm and used as a precursor to produce char. Proximate analysis of longan seed is shown in Table 2. The fixed carbon content of this seed is 19.6% with relatively low ash content and high volatile content. The fixed carbon is comparable with the other carbonaceous materials such as apricot stone, almond shell, grape seed and oil palm stone, as reported in the literature [25,26]. The precursor was carbonized in a horizontal tube furnace (Carbolite, UK) under the nitrogen atmosphere with a flow rate of 100 cc min^{-1}. Carbonizing temperature was increased from room temperature to 650 °C at a heating rate of 5 °C min^{-1} and then held at this temperature for 2 h. The proximate analysis of the resultant char is also shown in Table 2. The fixed carbon content was increased to 86.1% due to the removal of volatiles and tars from the seed.

3.2. Gasification of char and activated carbon characterization

The char was gasified in a horizontal tube furnace using carbon dioxide (Linde Gas, 99.95%) as a gasifying agent. The range of activation temperature was 750–900 °C and the holding time was between 30–180 min, giving burn-off up to 90%. The porous properties of the derived activated carbons were measured by nitrogen adsorption at 77 K using an Accelerated Surface Area and Porosimetry Analyzer (ASAP2010, Micromeritics, USA).

Table 2
Proximate analyses of longan seed and char

Sample	Proximate analysis (dry basis), wt%		
	Fixed carbon	Volatile matter	Ash
Longan seed	19.6	78.7	1.7
Longan seed-derived char	86.1	9.4	4.5

4. Results and discussions

The nitrogen adsorption isotherms of some activated carbons obtained at different burn-off are shown in Fig. 2. Nitrogen adsorption capacity increases with an increasing in the burn-off extent and then it decreases at the highest burn-off of 90.1%. The isotherms show type I at low burn-off and change to type IV isotherm at burn-offs higher than 46%. The size of the hysteresis loop appears to increase with increasing in burn-off, indicating an increased proportion of mesopore volume. The porous properties of activated carbons prepared at different burn-off are summarized in Table 3. The values of BET surface area, total pore volume and the micropore volume, increase with increasing in burn-off in the range from 10% to 70%, beyond which they decrease with higher burn-off. These activated carbons are dominated with microporosity which is shown by the high percentage of micropore volume of greater than 70%.

The structural model proposed in this paper is tested against the experimental gasification data of the longan seed-derived char. The BET surface area and total pore volume are used as the criteria to validate the model. As the model is constructed to describe only the gasification process, the physical properties of raw char will provide the initial conditions for the model. These initial parameters are surface area and total pore volume of char, and their values are 300 $m^2 g^{-1}$ and 0.14 cc g^{-1}, respectively.

From the characteristic of this structural model, the porosity is evolved due to the partial consumption of carbon layers, and the space between layers will constitute a pore, from which we can readily determine its pore volume and geometrical surface area. Since we assign only 15 layers initially in each graphitic crystallite, the largest possible pore width is 46.9 Å, in which we

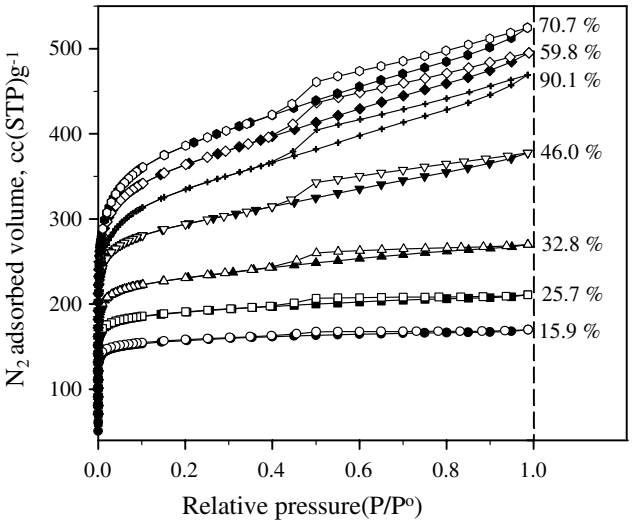

Fig. 2. Experimental nitrogen adsorption isotherms at 77 K for some activated carbons prepared at different char burn-offs.

Table 3
Experimental porous properties of longan seed based-activated carbon prepared at different char burn-offs

%Burn-off	BET surface area ($m^2 g^{-1}$)	Total pore volume ($cc g^{-1}$)	Micropore volume ($cc g^{-1}$)	Meso- and macropore volume ($cc g^{-1}$)	%Micropore volume
10.4	443	0.21	0.21	0.00	100
14.0	451	0.22	0.21	0.01	95
15.9	521	0.26	0.24	0.02	92
18.7	538	0.27	0.25	0.02	92
25.7	631	0.33	0.29	0.04	87
25.8	705	0.37	0.32	0.05	86
32.8	766	0.42	0.35	0.07	83
35.6	813	0.45	0.38	0.07	84
46.0	975	0.58	0.45	0.13	77
48.9	1035	0.62	0.49	0.13	79
59.8	1204	0.76	0.56	0.20	73
70.7	1278	0.81	0.60	0.21	74
90.1	1108	0.73	0.52	0.21	71

have assumed that the interlayer spacing between the two adjacent graphite layers is 3.35 Å. Thus, our model is restricted only to the description of micropores and lower end of the mesopore range. To facilitate the discussion later we shall define fine pores are those having widths smaller than 10 Å, large pores for widths greater than 20 Å and medium pores are those in between.

The evolution of surface area and total pore volume versus the extent of the gasification obtained from our structural model is shown in Fig. 3 as solid lines with unfilled symbols. Experimental data are also shown in the same figure as solid symbols. The description of the surface area is regarded as excellent while that of pore volume is reasonably adequate despite the simplicity of our structural model. The model correctly describes the trend of the evolution of surface area and pore volume, in the sense that they both increase with burn-off and then decrease once a threshold burn-off has been reached. The agreement between the simulated pore volume and the data is good up to 25% burn-off, beyond which the model underpredicts the data. Furthermore, the maximum in the pore volume observed experimentally occurs at about 70% burn-off, while the model predicts a value of 85%. Nevertheless, the maximum value of the pore volume obtained by the model, $0.86\ cc g^{-1}$, agrees fairly well with the experimental data of $0.81\ cc g^{-1}$. Given the fact that the surface area is well described by the model and the pore volume only reasonably described, we can postulate that the spacing between the two initial adjacent graphite-like layers should be greater than 3.35 Å. This is a possible reason why there is an underestimation of the total pore volume while the surface area is excellently described. This argument is physically justified as the interlayer spacing of 3.35 Å is for perfect parallel graphite layers. For graphene layers in activated carbon, which are known to be turbostratic, the spacing between two layers would be expected to be greater than 3.35 Å. As the burn-off is greater than 90%, the pore volume predicted by the model is higher than the experimental data and this is most likely due to the possible fact that the solid is disintegrated at this

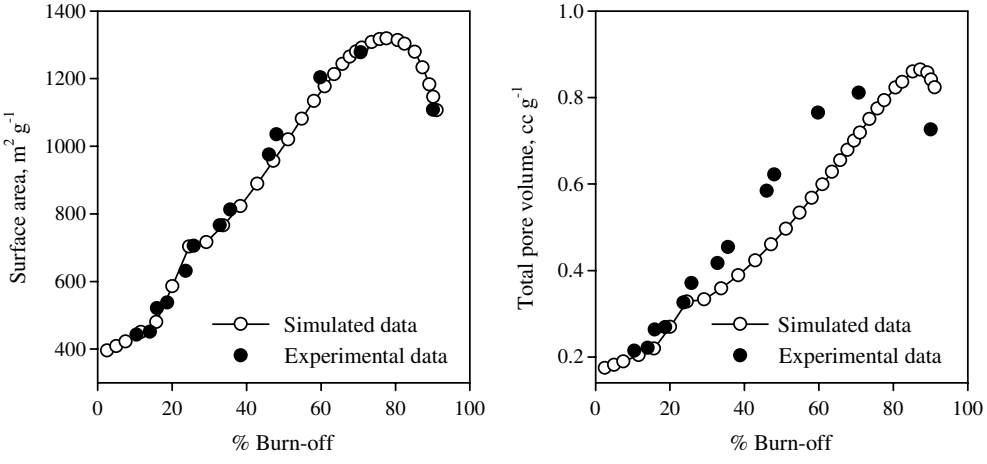

Fig. 3. Surface area and total pore volume of experimental and simulated data.

high burn-off and as a result the actual pore volume is lower than that predicted by the model.

To check the effect of interlayer spacing, the simulation was also performed with two interlayer spacings of 3.70 and 4.50 Å. The first value is the one suggested by Franklin [27] for the interlayer spacing of a non-graphitizing carbon. Since the gasification was simulated with the same set of reactivities, the change would occur only for the pore volume but not with the surface area evolution. Fig. 4 shows the simulated total pore volume and micropore volume for different interlayer spacings, as compared with the experimental data. The increasing of interlayer spacing shifts the pore volume curve upward closer to the experimental points. From the results, the interlayer spacing of 4.5 Å provides excellent agreement up to 60% burn-off for the total pore volume and very good agreement for the micropore volume over the entire range of burn-off. Therefore, it could be inferred from the simulation that the interlayer spacing of the graphitic crystallite of longan seed derived char should probably have a value of 4.50 Å.

Apart from the surface area and the pore volume that can be obtained from the model, information about the pore size distribution of the gasified carbon can also be derived. This is shown in Fig. 5 for a number of burn-off and this pore evolution data are also presented as pore volume for each pore size range (Table 4). The results show a deeper insight on how pores are generated and their pore sizes are evolved with the degree of burn-off. There are three stages of pore development that can be observed in Fig. 5. The first stage is for burn-off less than 5%, the second stage is for burn-off between 5% to 60% and finally the third stage for burn-off higher than 60%. During the first stage, only fine pores were evolved (creation stage), and the volume of these pores increases with burn-off as reflected in Fig. 5 in that the volume increases while the pore width remains constant. These fine pores result from the increase in the number

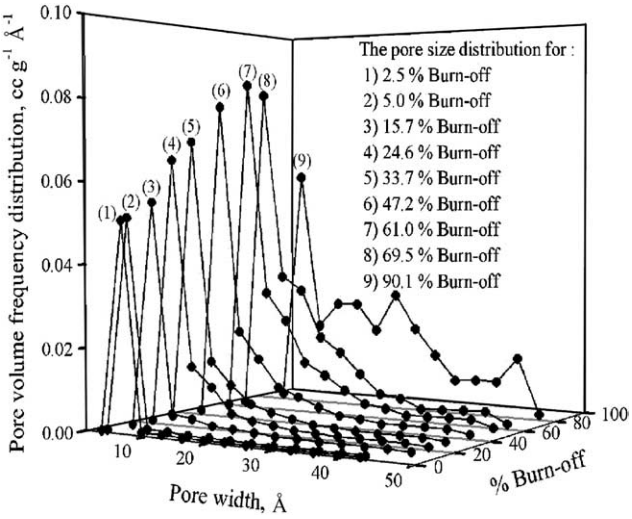

Fig. 5. The pore size distribution of simulated data at different degrees of char burn-offs.

of these pores as well as the increase in the length of the existing fine pores. In the second stage, fine pores are still continually created, and there is the onset of the medium pores. The main mechanism in this period is the increase in the length of each pore, which is due to the consumption of carbon layers, resulting in larger volume and surface area but the pore size remains fairly constant. In the last stage, the volume of fine pores decreases but the medium and large pores continue to evolve at the expense of fine pores. In this stage, two processes are possible. The first one is the coalescence of smaller pores to form larger pores and the collapse of pores due to the complete removal of the pore walls of some pores. The coalescence occurs in the early period of the third stage, and mechanistically this happens when one or two layers separating the two adjacent pores are completely consumed, resulting in the coalescence of these two pores into a larger one. Associated

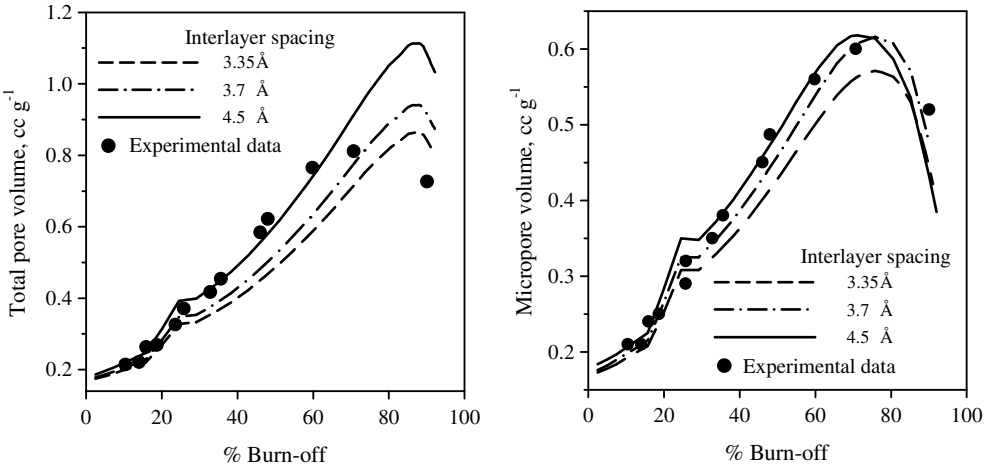

Fig. 4. Total pore and micropore volumes of experimental and simulated results with different interlayer spacing.

Table 4
Model-generated pore evolution data

%Burn-off	Total pore volume ($cc\,g^{-1}$)	Fine and medium pores (6.7–20 Å) volume ($cc\,g^{-1}$)	Large pores (20–46.9 Å)
2.5	0.175	0.173	0.002
5.0	0.182	0.179	0.003
15.7	0.22	0.21	0.01
24.6	0.33	0.31	0.02
33.7	0.36	0.33	0.03
47.2	0.46	0.41	0.05
61.0	0.60	0.51	0.09
69.5	0.70	0.56	0.14
90.1	0.84	0.44	0.40

with this phenomenon is the loss of surface area but the volume and porosity increase. The collapse of pores occurs at the end of the third stage, and as a result pore volume, and surface area decrease with burn-off as seen experimentally in Fig. 3 for burn-off greater than 80%. These results are in line with the results found by Dubinin and Zaverina [28], from which it was reported that at burn-off less than 50% the porous structure of activated carbon is highly microporous, at burn-off lying between 50% and 75% the product carbon contains all types of pores, micro, meso and macropores, and at burn-off higher than 75% the porous structure is dominated with macropores.

The DFT and simulated pore size distributions (PSD) of gasified carbon at two levels of char burn-offs are compared as shown in Fig. 6. The DFT-derived PSD results were calculated from nitrogen adsorption isotherm data using the standard DFT (Density Functional Theory) method supplied by Micromeritics as DFT Plus software (solid lines). There are two distinct peaks for the experimental PSD at pore width of 7 and 11 Å, respectively. The simulated PSD show a broader distribution into a smaller size range and give the second peak only at higher burn-off of 90.1%. One possible reason for this is that smaller pores could not be probed by nitrogen adsorption because these pores are either too small for nitrogen molecules to enter or the diffusional resistances at 77 K are too great to be probed within reasonable equilibration time. As shown in Fig. 6, the maximum value of pore volume distribution occurs at about 5 and 7 Å for the simulated and experimental PSD, respectively, with the former giving the value about four times less than the latter. However, the experimental and simulated total pore volume compare fairly well, respectively, 0.59 versus 0.46 $cc\,g^{-1}$ (47.2% burn-off) and 0.73 versus 0.84 $cc\,g^{-1}$ (90.1% burn-off). Generally speaking, pore size distributions derived from the two techniques are within the same size range, although the simulation results give smaller average pore size as compared to the experimental estimation.

5. Conclusions

The results presented in this paper show that the developed structural model for carbon activation offers the significant advantage to explore the extent of gasification of char. The valuable information of surface area, total pore volume and pore size distribution are directly obtained from this model. The model results are tested

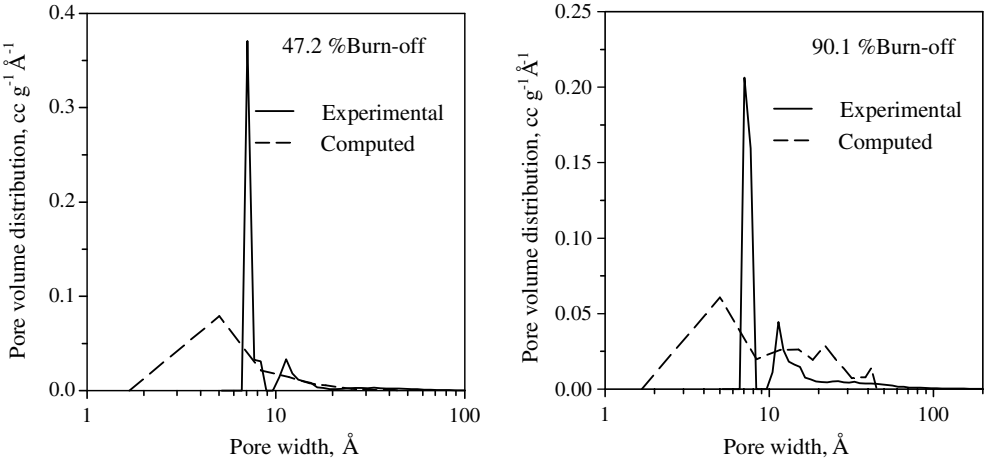

Fig. 6. Comparison of experimental and computed pore size distributions of activated carbon at two degrees of char burn-offs.

against the experimental data of longan fruit seed char gasification with carbon dioxide, and it was found that the description of surface area is regarded as excellent while that of pore volume is adequate. The mechanism for pore evolution during gasification process is proposed as a three-stage development, in which pore creation, pore coalescence and pore collapse contribute to different extent in each of those three stages. From this model results, it is also found that the optimum interlayer spacing of adjacent layer in a carbon crystallite of a carbon char derived from longan seed should probably be 4.5 Å.

Acknowledgement

Support of Royal Golden Jubilee PhD program from Thailand Research Fund(TRF) is gratefully acknowledged.

References

[1] El-Merraoui M, Aoshima M, Kaneko K. Micropore size distribution of activated carbon fiber using the density functional theory and other methods. Langmuir 2000;16(9):4300–4.
[2] Gavalda S, Gubbins KE, Hanzawa Y, Kaneko K, Thomson KT. Nitrogen adsorption in carbon aerogels: A molecular simulation study. Langmuir 2002;18(6):2141–51.
[3] Suzuki T, Iiyama T, Gubbins KE, Kaneko K. Quasi-symmetry structure of CCl_4 molecular assemblies in a graphitic nanopore: A grand canonical Monte Carlo simulation. Langmuir 1999;15(18): 5870–5.
[4] Gavalda S, Kaneko K, Thomson KT, Gubbins KE. Molecular modeling of carbon aerogels. Colloids and surfaces A: Physicochemical and engineering aspects 2001;187–188:531–8.
[5] Ohba T, Suzuki T, Kaneko K. Relationship between DR-plot and micropore width distribution from GCMC simulation. Carbon 2000;38(13):1892–6.
[6] Wang ZM, Kaneko K. Effect of pore width on micropore filling mechanism of SO_2 in carbon micropores. J Phys Chem B 1998;102(16):2863–8.
[7] Kaneko K. Nanospace geometry-sensitive molecular assembly. Supramol Sci 1998;5(3–4):267–73.
[8] El-Merraoui M, Tamai H, Yasuda H, Kanata T, Mondori J, Nadai K, et al. Pore structures of activated carbon fibers from organometallics/pitch composites by nitrogen adsorption. Carbon 1998;36(12):1769–76.
[9] Setoyama N, Suzuki T, Kaneko K. Simulation study on the relationship between a high resolution α_S-plot and the pore size distribution for activated carbon. Carbon 1998;36(10):1459–67.
[10] Kruk M, Jaroniec M, Choma J. Comparative analysis of simple and advanced sorption methods for assessment of microporosity in activated carbons. Carbon 1998;36(10):1447–58.
[11] Li Z, Kruk M, Jaroniec M, Ryu SK. Characterization of structural and surface properties of activated carbon fibers. J Colloid Interface Sci 1998;204(1):151–6.
[12] Jaroniec M, Gilpin RK, Choma J. Correlation between microporosity and fractal dimension of active carbons. Carbon 1993; 31(2):325–31.
[13] Jaroniec M, Madey R, Choma J, McEnaney B, Mays TJ. Comparison of adsorption methods for characterizing the microporosity of activated carbons. Carbon 1989;27(1):77–83.
[14] Abe M, Kawashima K, Kozawa K, Sakai H, Kaneko K. Amination of activated carbon and adsorption characteristics of its aminated surface. Langmuir 2000;16(11):5059–63.
[15] Do DD. Adsorption analysis: equilibria and kinetics. New Jersey: Imperial College Press; 1998.
[16] Petersen EE. Reaction of porous solid. AIChE J 1957;3(4):443–8.
[17] Szekely J, Evans JW. A structural model for gas–solid reactions with a moving boundary. Chem Engng Sci 1970;25:1091–107.
[18] Hashimoto K, Silveston PL. Gasification: Part I. Isothermal, kinetic control model for a solid with a pore size distribution. AIChE J 1973;19(2):259–67.
[19] Gavalas GR. A random capillary model with application to char gasification at chemically controlled rates. AIChE J 1980;26(4): 577–85.
[20] Bhatia SK, Perlmutter DD. A random pore model for fluid-solid reactions: I. Isothermal, kinetic control. AIChE J 1980;26(3): 379–85.
[21] Sandmann Jr CW, Zygourakis K. Evolution of pore structure during gas–solid reactions: Discrete models. Chem Engng Sci 1986;41(4):733–9.
[22] Bansal RC, Donnet J-B, Stoeckli F. Active carbon. New York: Marcel Dekker; 1988.
[23] Byrne JF, Marsh H. Introductory overview. In: Patrick JW, editor. Porosity in carbons: characterization and applications. London: Edward Arnold; 1995. p. 2–48.
[24] Franklin RE. The structure of graphitic carbons. Acta Cryst 1951;4:253–61.
[25] Guo J, Lua AC. Preparation of activated carbons from oil-palm-stone chars by microwave-induced carbon dioxide activation. Carbon 2000;38:1985–93.
[26] Gergova K, Petrov N, Eser S. Adsorption properties and microstructure of activated carbons produced from agricultural by-products by steam pyrolysis. Carbon 1994;32(4):693–702.
[27] Franklin RE. The interpretation of diffuse X-ray diagrams of carbon. Acta Cryst 1950;3:107–21.
[28] Dubinin MM, Zaverina ED. Dokl Akad Nauk SSSR 1949;68: 91–4.